Journal of Alloys and Compounds, 191 (1993) 243–249
JALCOM 501

Hydrogen-induced transformation to an amorphous state in the Laves phases Ce(Ru, M)$_2$ (M ≡ Fe, Co, Ni)

Yong-Gyoo Kim and Jai-Young Lee
Department of Materials Science and Engineering, Korea Advanced Institute of Science and Technology, Kusong-Dong 373-1, Yusung-Gu, Taejon (South Korea)

(Received April 24, 1992; in final form August 31, 1992)

Abstract

The structural changes of the Laves phases Ce(Ru$_{1-x}$M$_x$)$_2$, where $x = 0.05$–0.25 and M is the transition elements, such as Fe, Co and Ni, during hydrogen absorption are investigated through X-ray diffraction (XRD), transmission electron microscopy and differential scanning calorimetry (DSC). All the examined ternary alloys, regardless of the composition and the species of the third elements, can be amorphized by hydrogen absorption at room temperature, even though the binary CeRu$_2$ alloy absorbs hydrogen in the crystalline hydride state. The amorphization mechanism is suggested to be identical to that of the binary CeM$_2$ Laves phases, indicating that the elastic strain caused by hydrogen plays a key role in the amorphization. The critical strain applied on the Ce(Ru$_{0.75}$Ni$_{0.25}$)$_2$ compound prior to amorphization is calculated through the DSC and XRD analysis, and it is about 1.9 ± 0.5 vol.%. It is proposed that the distinct change in the hydrogenation properties of the CeRu$_2$ system by this substitution is caused by the build-up of the lattice distortion owing to the presence of the third element, which has a smaller atomic radius.

1. Introduction

It is well known that hydrogen absorption in some intermetallic compounds induces a transformation to an amorphous state, *i.e.* hydrogen-induced amorphization (HIA) [1]. The Laves phases with C15 cubic structure composed of rare earth elements and transition metals are the representative system of HIA [2, 3]. A number of Laves phases are reported to be amorphized at some elevated temperatures of 200–300 °C, which indicates a thermally activated process. Er-base compounds are an example of the above process [4]. However, Ce-base systems, such as CeNi$_2$, show amorphization reactions by hydrogenation treatment at or below room temperature [5]. These resemble the athermal martensitic transformation. These two different mechanisms have recently been explained to be caused by the difference in the elastic moduli of the compound [6, 7]. At a given charging condition, a compound with a relatively high elastic modulus can maintain its crystalline structure but a compound with a low modulus value does not form a crystalline hydride phase. In other words, the elastic modulus can be regarded as the resistance to lattice expansion during hydrogen absorption.

Among the Ce-base Laves phases, CeRu$_2$ with C15 structure has a higher modulus than those of other CeM$_2$ compounds, where M is Fe, Co or Ni. CeRu$_2$ can absorb hydrogen in the crystalline state at room temperature [8] and, because of the high modulus of CeRu$_2$, it can maintain the crystalline state during hydrogen absorption. Recently, it has been reported that the hydrogenated crystalline CeRu$_2$H$_5$ phase can be amorphized by partial hydrogen desorption at room temperature [9]. This reaction is the reverse of the common hydrogen-induced amorphization phenomenon. It is suggested that the amorphization mechanisms of the above two processes are similar in aspects of the elastic instability of the compounds owing to the elastic strain accumulation causing the collapse of the lattice during the hydrogen absorption or desorption process.

The purpose of this study is to investigate the hydrogen absorption or desorption behaviors of pseudobinary Ce(Ru, M)$_2$ alloys, where M is a transition element, such as Fe, Co or Ni. The addition of small amounts of a third element may give rise to a change in the hydrogenation behaviors. In this work, it is found that hydrogen absorption in Ce(Ru, M)$_2$ induces amorphization at room temperature. The role of the alloying element and the amorphization mechanism are discussed on the basis of the observed experimental results.

0925-8388/93/$6.00

2. Experimental details

The pseudobinary Laves phases $Ce(Ru_{1-x}M_x)_2$ ($x = 0.05$–0.25; M = Fe, Co, Ni) were prepared by arc melting in an Ar atmosphere. The button-type ingots were crushed into powder below 100 mesh in air, and then checked by X-ray diffractometry (XRD) using Cu Kα radiation. In Fig. 1, XRD patterns of the as-received $Ce(Ru_{0.75}M_{0.25})_2$ alloys before and after substitution are shown for example. All the samples prepared in this work exhibit the C15 cubic Laves structure.

Hydrogen absorption treatments were carried out in a conventional volumetric apparatus. The high purity hydrogen gas (99.999%) was inserted into the sample. The charging pressure, temperature and time were fixed at 50 atm H_2, room temperature and 24 h respectively. After hydrogenation, the structural changes in the samples were checked by XRD.

To examine the thermal behavior of the hydrogenated samples, differential scanning calorimetry (DSC) was performed using a Perkin–Elmer DSC-4 unit in an Ar atmosphere. Selected samples were quenched to room temperature in the DSC unit with a cooling rate of 320 K min^{-1} for XRD analysis.

To confirm the amorphous state, the microstructure of the hydrogenated sample was investigated using transmission electron microscopy (TEM). The TEM sample was prepared by crushing in acetone.

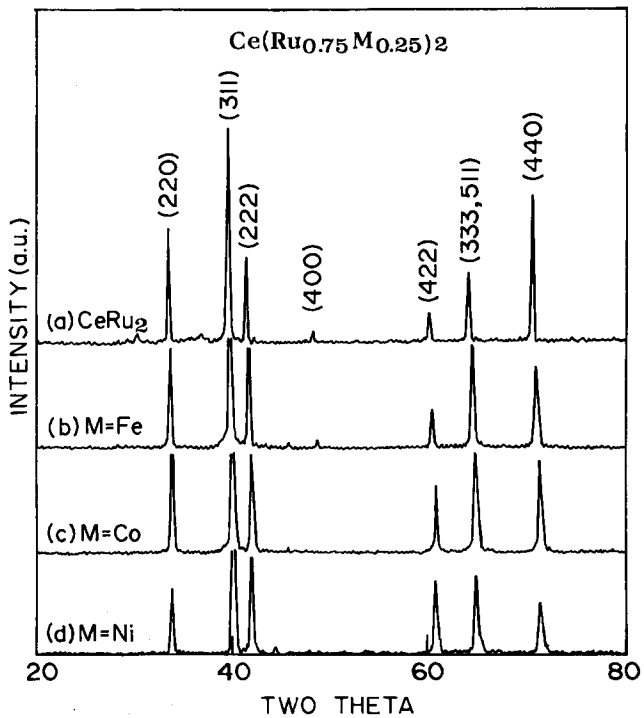

Fig. 1. XRD patterns of the $Ce(Ru_{0.75}M_{0.25})_2$ before and after the substitution.

3. Results and discussion

In Table 1, the crystallographic data of $Ce(Ru_{1-x}M_x)_2$ are summarized. The as-received samples exhibit the C15 cubic Laves structure for all compositions. As the third elements are added, the lattice parameters gradually decrease owing to the smaller atomic radii of M than that of Ru. From the alloy phase diagram [10], it is known that the solubilities of the transition elements Fe, Co and Ni in Ce are very small. However, Ru forms a solid solution over a wide range of compositions with the transition elements. In the case of Ru and Co, they form a homogeneous solid solution over the whole composition range at ambient temperature. Thus, it is thought that the substituted transition element entirely occupies the Ru sites.

Figure 2 shows the XRD patterns of the $Ce(Ru_{1-x}Ni_x)_2$ hydrogenated at room temperature. By hydrogen absorption, all the Bragg reflections disappear and only broad maxima develop. This indicates intuitively that amorphous phases are formed, and the very small compositional modification in the host compound of $CeRu_2$ results in HIA even at room temperature. In Fig. 3, the structural changes in $Ce(Ru_{0.75}M_{0.25})_2$

TABLE 1. Crystallographic data of $Ce(Ru_{1-x}M_x)_2$ pseudobinary Laves phases

M≡Ni		M≡Co		M≡Fe	
x	a (Å)	x	a (Å)	x	a (Å)
0.00	7.555	0.25	7.462	0.25	7.512
0.05	7.525				
0.15	7.472				
0.25	7.452				

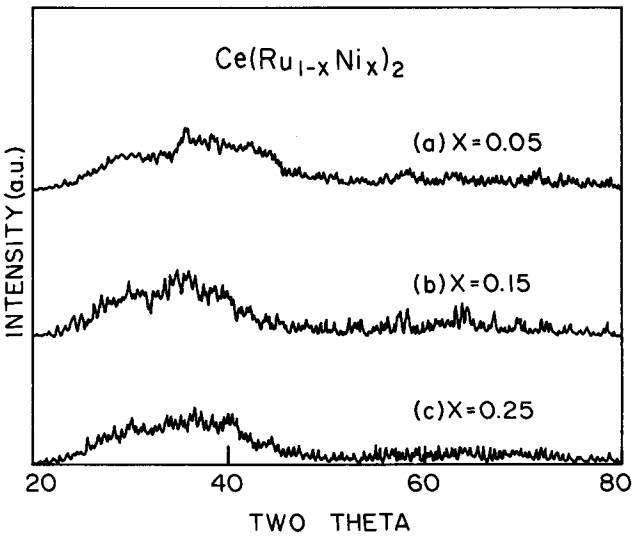

Fig. 2. XRD patterns of the $Ce(Ru_{1-x}Ni_x)_2$ hydrogenated at room temperature with the Ni composition.

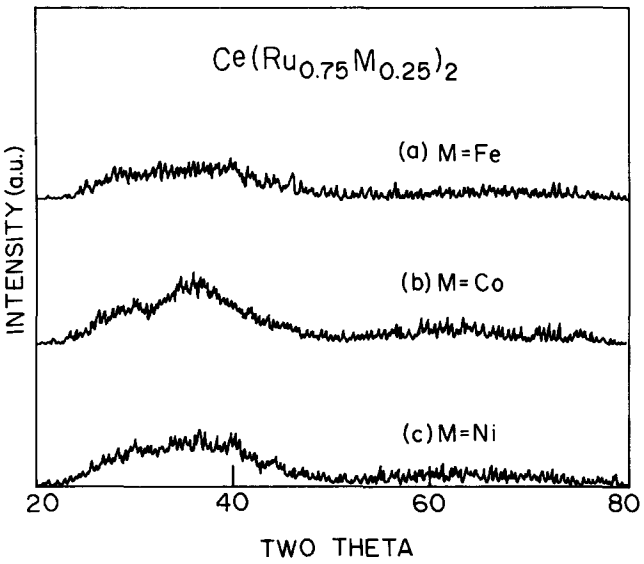

Fig. 3. XRD patterns of the $Ce(Ru_{0.75}M_{0.25})_2$ hydrogenated at room temperature with the transition elements.

alloys during hydrogen absorption are shown, so that they all can be amorphized at room temperature. The above results (Figs. 2 and 3) imply that HIA in this alloy system is not affected by the species within the investigated composition range ($x=0.05$–0.25) of the third elements. Thus, the experimental work and analysis on the $Ce(Ru_{0.75}Ni_{0.25})_2$ system will be mainly presented in this report.

To confirm whether the broad maximum observed in the XRD pattern corresponds to an amorphous phase or not, TEM work has been performed on the $Ce(Ru_{0.75}Ni_{0.25})_2H_x$ sample shown in Fig. 4(a). In the bright-field image, there is no crystalline contrast but a mottled structure is observed. The electron diffraction pattern (Fig. 4(b)) shows the diffuse halo ring, which is a typical pattern of an amorphous material. Therefore, it is certain that $Ce(Ru_{0.75}Ni_{0.25})_2$ is amorphized completely by hydrogen absorption.

In these experimental conditions, the crystalline hydride phases are not observed in all the systems examined. For example, the XRD patterns of the $Ce(Ru_{0.75}Ni_{0.25})_2$ compound with different hydrogen contents are shown in Fig. 5. At $H/M=0.7$, a broad maximum pattern is developed at around 2θ-28°–43°. The sharp diffraction peaks are those of the unreacted and as-received $Ce(Ru_{0.75}Ni_{0.25})_2$ phase. In other words, the only hydrogenated region is converted to an amorphous phase, and the amorphous and crystalline phases are clearly distinguished from each other. Hydrogen is not in solution in an amount measurable by XRD analysis. Therefore, it is certain that the amorphization behaviors of $Ce(Ru_{1-x}M_x)_2$ are very similar to the case of the $CeNi_2$ system [5] in the sense that direct amorphization reactions during hydrogen absorption take

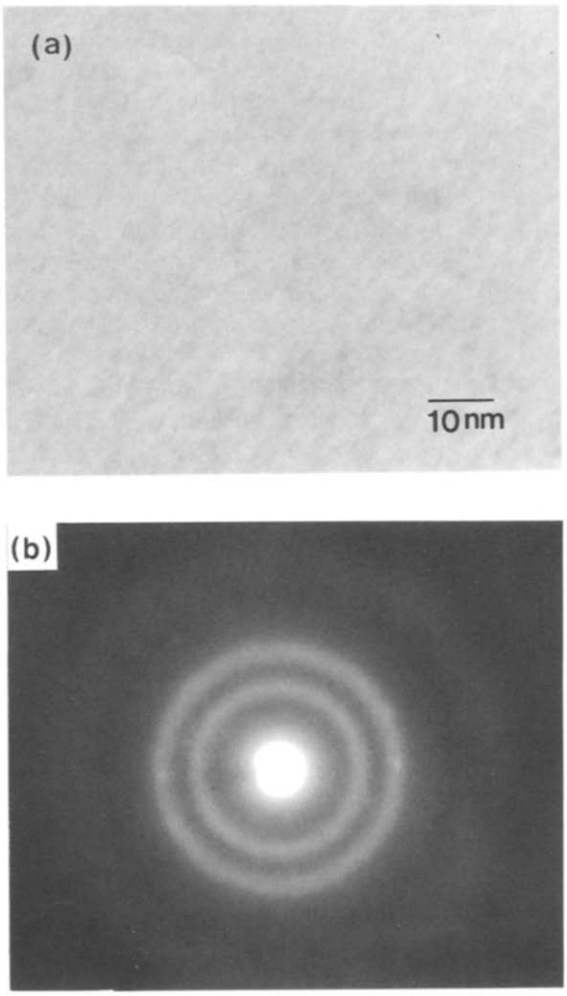

Fig. 4. (a) Transmission electron micrograph and (b) the corresponding electron diffraction pattern for the $Ce(Ru_{0.75}Ni_{0.25})_2H_x$ hydrogenated at room temperature.

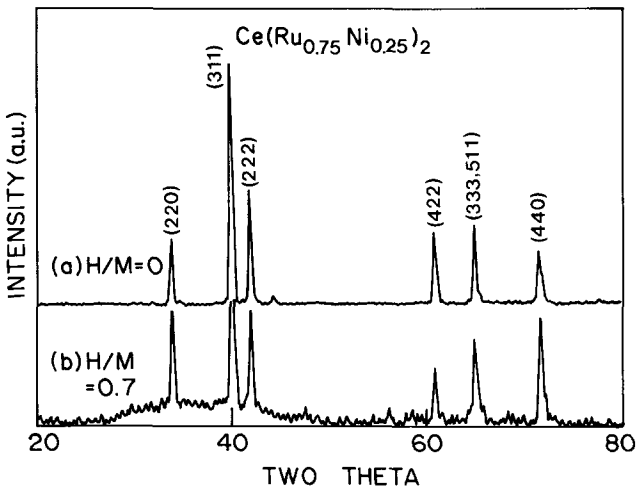

Fig. 5. XRD patterns of the $Ce(Ru_{0.75}Ni_{0.25})_2$ with the different hydrogen contents.

place in both cases. Recently, the amorphization mechanisms during hydrogen absorption in the RM_2 (R≡rare earths, M≡Fe, Co, Ni) Laves phases have been classified into two groups relative to the possibility of crystalline hydride formation; one group is the thermally activated process caused by the short-range motion of the transition elements, and the other group is the athermal process triggered by the elastic strain owing to hydrogen absorption [6, 7]. The Ce-base alloys, including this $Ce(Ru_{1-x}M_x)_2$ system, follow the athermal process, implying that the reaction mechanism is the same in each case.

In Fig. 6, the DSC results for the amorphous $Ce(Ru_{0.75}Ni_{0.25})_2H_x$ are shown. An endothermic reaction starts from the rather low temperature range (about 120 °C) and it forms a peak at 400 °C. To investigate the structural change in the sample relative to the endothermic peak, the samples are quenched from the temperature indicated by arrows and then checked by XRD. The results are shown in Fig. 7. Before the peak, broad maxima are still shown and thus it seems to be still mostly amorphous. After the endothermic reaction, a crystalline phase is observed and it is indexed to the $Ce(Ru_{0.75}Ni_{0.25})_2$ phase. The amorphous phase has crystallized into the original compound owing to the hydrogen release.

Generally, hydrogen evolution from the sample is shown as an endothermic reaction in a DSC curve. To confirm that the DSC curve shown in Fig. 6 is the result of hydrogen evolution, a hydrogen thermal desorption technique is adopted [11, 12]. By this method, the hydrogen evolution rate *vs.* temperature relationship is obtained. The amount of hydrogen desorbed is quantitatively calculated using gas chromatography (GC), when the sample is heated with a constant heating rate of 3 K min^{-1}. In Fig. 8, the hydrogen thermal desorption

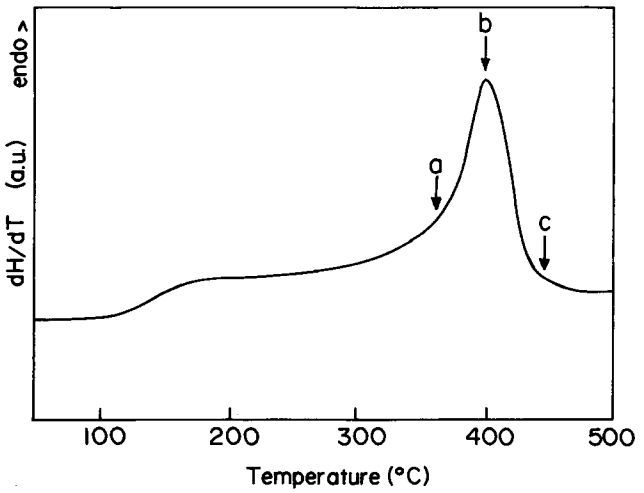

Fig. 6. Typical DSC curve for the amorphous $Ce(Ru_{0.75}Ni_{0.25})_2H_x$ hydrogenated at room temperature (heating rate 40 K min^{-1}).

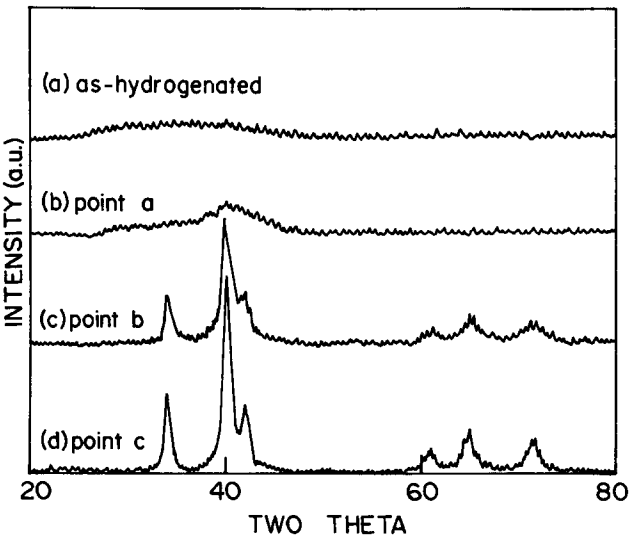

Fig. 7. XRD patterns of the $Ce(Ru_{0.75}Ni_{0.25})_2$ hydrogenated at room temperature and quenched in the DSC unit from the temperatures indicated by arrows in Fig. 6.

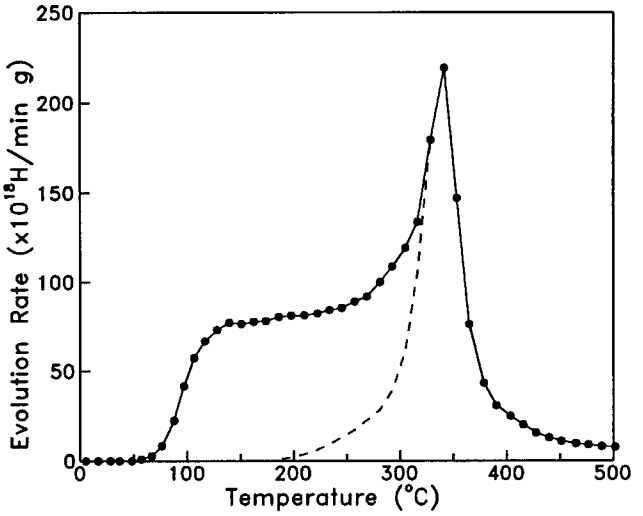

Fig. 8. Hydrogen thermal desorption spectrum of the amorphous $Ce(Ru_{0.75}Ni_{0.25})_2H_x$ with a heating rate of 3 K min^{-1}. The dotted line is the separation of the endothermic peak, assuming the Gaussian distribution function.

curve for the amorphous $Ce(Ru_{0.75}Ni_{0.25})_2H_x$ is shown. The peak area and temperature indicate the total desorbed hydrogen content and the energy level of hydrogen occupied in the matrix respectively. The desorbed hydrogen content in this sample is H/M = 5.0, *i.e.* $Ce(Ru_{0.75}Ni_{0.25})_2H_5$. This value is the same as that of $CeRu_2$. When comparing Figs. 6 and 8, the DSC and hydrogen desorption curves are very similar to each other in their peak shape, indicating that the DSC curve is caused by hydrogen desorption from the sample. In Fig. 8, the broken line is the calculated hydrogen evolution peak during the crystallization reaction found by assuming the Gaussian function. The fraction of hydrogen desorbed during crystallization is calculated

to be about 53% of the total hydrogen content. This amount of hydrogen remaining in the matrix is thought to be the minimum content for maintaining the amorphous structure, and it is effused during the crystallization process.

It should be noted that the crystallization process of amorphous $Ce(Ru_{0.75}Ni_{0.25})_2H_5$ is a single step. At the mid-stage of the reaction (for example, at point b in Fig. 5), the sample is a two-phase mixture of amorphous and crystallized phases. Hydrogen in the crystalline phase may be in the solid solution state. The solute hydrogen must generate the elastic strain in the lattice, and the degree of elastic strain in the crystalline matrix will be a critical factor for preserving the crystal structure.

In an XRD pattern, the diffraction peaks are broadened when an inhomogeneous elastic strain is present. In this work, the peak width variation of the (311) diffraction peak, which is the main diffraction plane of the C15 Laves phases, is investigated. In Fig. 9, the endothermic peak in the DSC curve is enlarged and the variation in the full width at half-maximum (FWHM) of the (311) diffraction peak, obtained from the samples quenched in the DSC unit from the temperatures indicated by arrows, is shown as a function of the quenching temperature. The FWHM has a nearly constant value up to the peak temperature and then it decreases gradually as the temperature increases. The crystallized regions formed in the early stage of crystallization will grow as the temperature increases. Thus the decrease in the FWHM surely is caused by the crystal growth in the higher temperature range above the peak temperature. The critical strain is thus calculated using the sample quenched from the peak temperature, showing a constant FWHM value.

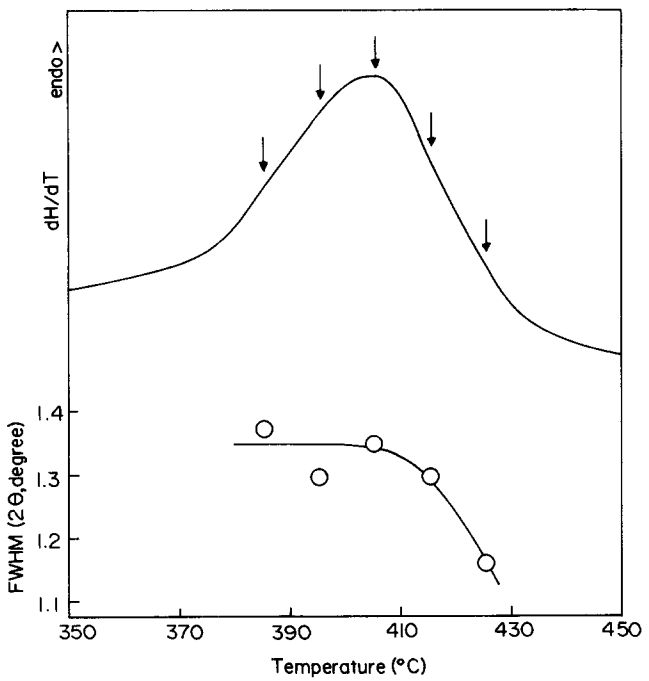

Fig. 9. Variation of the FWHM of the (311) reflection peak of the crystallized $Ce(Ru_{0.75}Ni_{0.25})_2$ samples obtained by rapid quenching from the temperatures indicated by arrows in the enlarged DSC curve, which is the endothermic peak shown in Fig. 6.

The degree of peak broadening in an XRD pattern is known to be caused by the lattice distortion and the fine crystallite size [13]. According to Wilson [14], the peak broadening $(\delta S_i)^D$ owing to lattice distortion is expressed in terms of S $(=2 \sin \theta/\lambda)$ as

$$(\delta S_i)^D = 2eS = 2e/d_{hkl} \quad (1)$$

where λ is the wavelength (-1.5406 Å), θ the Bragg angle in degrees, d the interplanar spacing and e the elastic strain $(\Delta d/d)$. The subscript i denotes the integral width of the peak and superscript D the distortion. The elastic strain $e(=\Delta d/d)$ is ambiguously defined as the upper limit of the lattice distortion. Representing eqn. (1) using 2θ, from $\delta S = 2 \cos\theta\, \delta\theta/\lambda$ we obtain

$$(\delta 2\theta_i)^D = 4\, e \tan\theta \quad (2)$$

According to Scherrer's equation [15], the integral width of the diffraction patterns relative to the size of the minute crystallite is given by

$$(\delta 2\theta_i)^S = K\lambda/L \cos\theta \quad (3)$$

where L is the crystallite size and K is the Scherrer constant which depends on the crystal system and on the selection of the integral width or FWHM. It is common to use $K=1$ when the integral width is used. The superscript S denotes the crystallite size. If the broadening of the diffraction patterns owing to both size and distortion are superimposed, then the total peak broadening $(\delta S)^O$ observed in the XRD pattern is

$$(\delta S)^O = (\delta S)^D + (\delta S)^S \quad (4)$$

Substituting eqns. (1) and (3) into eqn. (4) using $\delta\theta = \lambda\delta S/2 \cos\theta$, we obtain

$$(\delta S)^O = 1/L + 2eS \quad (5)$$

where it is taken that $K=1$. From eqn. (5), the crystallite size L is obtained from the intercept of the vertical line and the maximum lattice distortion from the slope when plotting $(\delta S)^O$ *vs.* S. Figure 10 shows the plots of eqn. (8) for the samples quenched in the DSC tests and the as-received $Ce(Ru_{0.75}Ni_{0.25})_2$ compound. For comparison, the results are also plotted for the as-received $CeRu_2$ system. The results obtained are summarized in Table 2.

The crystallite size of the crystallized phase is the smallest out of the three systems. Lattice distortion, in turn, is nearly absent in the $CeRu_2$ system, though it increases dramatically as Ni is substituted in small

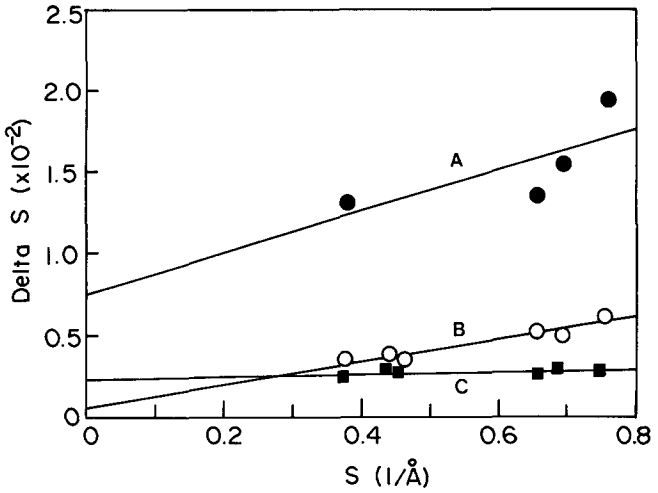

Fig. 10. Plots of integral width $(\delta S)^0$ *vs.* S. The line A is on the sample quenched in DSC unit from the peak temperature (point b in Fig. 6). The lines B and C are those of the as-received $Ce(Ru_{0.75}Ni_{0.25})_2$ and $CeRu_2$ respectively.

TABLE 2. Crystallite size and elastic strain calculated from the XRD analysis of the crystallized and as-received $Ce(Ru_{0.75}Ni_{0.25})_2$ compounds and the $CeRu_2$ system

	As-received $Ce(Ru_{0.75}Ni_{0.25})_2$	Crystallized $Ce(Ru_{0.75}Ni_{0.25})_2$	As-received $CeRu_2$
Crystallite size (Å)	1152	133	408
Elastic strain (%)	0.32	0.63	0.02

amounts. This increase is surely due to the smaller atomic radius of Ni than that of Ru. As the Ni is added into the lattice, the size mismatch may induce an inhomogeneous strain in the lattice. It is considered that the build-up of the lattice distortion would encourage the elastic collapse of the crystalline lattice, leading to amorphization.

Assuming that the lattice distortion of the crystallized phase is due only to the solute hydrogen atoms in the matrix, the critical strain for the transformation is $0.63 \pm 0.18\%$. When considering that the relation between the volume (ΔV) and line expansion (Δa) is approximately $\Delta V = 3\Delta a$, the volume strain is about $1.9 \pm 0.5\%$.

Previously, Linker reported that a critical strain value ($\Delta a/a$) for the crystal-to-glass transition during B implantation into thin Nb film was measured to be about 0.43% ($\Delta V = 1.3\%$), and the amorphization was accompanied by strain release [16]. The author argued the twofold role of the impurities in the amorphization process, namely that initially there is the build-up of strain on interstitial sites and then upon transformation the stabilization of the amorphous phase occurs. Hydrogen atoms also can be treated as impurities causing the strain in the matrix. The forced introduction of hydrogen into the lattice should result in severe elastic strain. If the strain exceeds a critical point, the crystalline structure would become mechanically unstable and transform into the amorphous state [7]. The maximum lattice dilatation as the result of disordering prior to amorphization for Kr^+-irradiated Zr_3Al was found to be 2.4 vol.% [17]. Moreover, during hydrogen absorption in Zr_3Al, the volume expansion was reported to be 2.4 vol.% by Meng *et al.* [18] and 2.0 vol.% by Lee *et al.* [19]. Our observed value is similar to the above values, indicating that volume expansion of around 2.0 vol.% is a common measure of the strain-induced amorphization of the compound, even though the solid state amorphizing techniques are different from each other.

4. Conclusions

With respect to hydrogen-induced amorphization in the $Ce(Ru_{1-x}M_x)_2$ system, where $x = 0.05$–0.25 and M is the transition elements, such as Fe, Co or Ni, the results can be summarized as follows.

(1) Hydrogen absorption in $Ce(Ru_{1-x}M_x)_2$ leads to amorphization even at room temperature.

(2) It is suggested that the elastic strain due to hydrogen absorption may collapse the crystalline lattice abruptly, such as in the case of the $CeNi_2$ system.

(3) The amorphous phase crystallizes into the original compound after partial desorption of hydrogen from the amorphous state.

(4) It is suggested that the role of the third element is the build-up of the elastic strain in the compound. This build-up of strain may contribute to the abrupt collapse of the crystalline lattice.

(5) From the DSC and XRD analysis of the crystallized $Ce(Ru_{0.75}Ni_{0.25})_2$, it is calculated that an elastic volume strain of about 1.9 ± 0.5 vol.% is applied to the lattice before the transformation to an amorphous state.

Acknowledgment

The financial support of the Korea Science and Engineering Foundation (KOSEF) is gratefully acknowledged.

References

1 X. L. Yeh, K. Samwer and W. L. Johnson, *Appl. Phys. Lett.*, *42* (1983) 242.
2 K. Aoki, T. Yamamoto and T. Masumoto, *Scr. Metall.*, *21* (1987) 27.
3 K. Aoki, A. Yanagitani, X. G. Li and T. Masumoto, *Mater. Sci. Eng.*, *97* (1988) 35.

4 U. I. Chung and J. Y. Lee, *Acta Metall., 38* (1990) 811.
5 Y. G. Kim, S. M. Lee and J. Y. Lee, *J. Less-Common Met., 169* (1991) 245.
6 U. I. Chung, Y. G. Kim and J. Y. Lee, *Philos. Mag. B, 63* (1991) 1119.
7 Y. G. Kim and J. Y. Lee, *J. Alloys Comp., 187* (1992) 1.
8 D. Fruchart, F. Vailiant, A. Rouault, A. Benoit and J. Flouquet, *J. Less-Common Met., 101* (1984) 285.
9 Y. G. Kim and J. Y. Lee, *Scr. Metall., 24* (1990) 2123.
10 E. A. Brandes (ed.), *Smithells Metals Reference Book,* 6th edn., Butterworth, Guildford, 1983.
11 H. G. Lee and J. Y. Lee, *Acta Metall., 32* (1984) 131.
12 G. W. Hong and J. Y. Lee, *Acta Metall., 32* (1984) 1581.
13 H. P. Klug and L. E. Alexander, *X-ray Diffraction Procedures for Polycrystalline and Amorphous Materials,* 2nd edn, Wiley, New York, 1974, p. 618.
14 A. J. C. Wilson, *Proc. Phys. Soc., London, 81* (1983) 41.
15 P. Scherrer, *Gött. Nachr., 2* (1918) 98.
16 G. Linker, *Solid State Commun., 57* (1986) 773.
17 P. R. Okamoto, L. E. Rehn, J. Pearson, R. Bhadra and M. Grimsditch, *J. Less-Common Met., 140* (1988) 231.
18 W. J. Meng, P. R. Okamoto, L. J. Thompson, B. J. Kestel and L. E. Rehn, *Appl. Phys. Lett., 53* (1988) 1820.
19 J. Y. Lee, W. C. Choi, Y. G. Kim and J. Y. Lee, *Acta Metall., 39* (1991) 1693.